






Investigation of $^{12-14}\text{C}$ isotopes via Tohsaki-Horiuchi-Schuck-Röpke wave function with cluster breaking

Songjie Li ¹, Mengjiao Lyu ^{2,*}, Zhongzhou Ren, ^{1,†} Qing Zhao ³, Songju Lei ⁴, Akihiro Tohsaki,⁵ Gerd Röpke ⁶, Hisashi Horiuchi,⁵ Chang Xu,⁷ Niu Wan,⁸ and Bo Zhou^{9,10}

¹*School of Physics Science and Engineering, Tongji University, Shanghai 200092, China*

²*College of Physics, Nanjing University of Aeronautics and Astronautics, Nanjing 210016, China*

³*School of Science, Huzhou University, Huzhou 313000, Zhejiang, China*

⁴*Chip and Algorithm Solution Department, Honor Device Company, Ltd., Shanghai 201203, China*

⁵*Research Center for Nuclear Physics (RCNP), Osaka University, Osaka 567-0047, Japan*

⁶*Institut für Physik, Universität Rostock, 18051 Rostock, Germany*

⁷*School of Physics, Nanjing University, Nanjing 210093, China*

⁸*School of Physics and Optoelectronics, South China University of Technology, Guangzhou 510641, China*

⁹*Institute of Modern Physics, Fudan University, Shanghai 200433, China*

¹⁰*Faculty of Science, Hokkaido University, Sapporo 060-0810, Japan*



(Received 10 April 2023; revised 12 March 2024; accepted 2 May 2024; published 31 May 2024)

We investigate the ground-state structures of $^{12-14}\text{C}$ isotopes, which exhibit the coexistence of the cluster and shell-like states, using the cluster breaking Tohsaki-Horiuchi-Schuck-Röpke (CB-THSR) wave function. This approach incorporates cluster breaking nucleon-nucleon pairs, making it particularly suitable for describing the cluster states that feature mixed configurations and dynamic cluster motion. Through variational optimization of THSR bases, we find the coupling between the motions of clusters and valence neutrons in different configurations of $^{12-14}\text{C}$ isotopes, e.g., dumbbell-like molecular orbits of valence neutrons coupled with an oblate $3-\alpha$ core, and a prolate $3-\alpha$ core surrounded by ringlike valence neutron distributions. For describing the coexistence of shell-like structures and cluster formation in the compact cores of $^{12-14}\text{C}$ isotopes, we introduce CB pairs into the THSR approach to formulate the CB-THSR wave function, which allows a further optimization of the variational wave function and the binding energy. The results suggest oblate and shell-like structures for the ground states of ^{12}C and $^{13-14}\text{C}$, respectively. As compared to the original THSR calculation, our new model yields relatively more accurate spectra for $^{12-14}\text{C}$ isotopes, as well as their matter rms radii. The improved results show that α clusters are broken by the CB pairs, and the CB-THSR wave functions describe a more compact spatial extension of cluster motion, while such strong overlaps between α clusters are not energetically favored in pure cluster models. Finally, we discuss the breaking of α clusters in $^{12-14}\text{C}$ isotopes via the calculations of momentum distributions and form factors, and it is found that both the particle exchange and the paired excitation should be included for describing the compact cluster states.

DOI: [10.1103/PhysRevC.109.054329](https://doi.org/10.1103/PhysRevC.109.054329)

I. INTRODUCTION

In atomic nuclei, nucleons are combined by the internucleon interactions, and various nuclear structures are constructed under the detailed balance between middle-range nuclear attraction, antisymmetrization, and short-range repulsion [1]. In nuclear structures, correlations between nucleons arise due to the saturation or short-range properties of the nucleon-nucleon force. Nuclear clusters, which are spatial aggregations of nucleons, are formed as subsystems in nuclei. Specifically, the α clusters are formed with very strong bindings due to the spin-isospin saturation in the internucleon interaction. Hence, multiple approaches considering

nuclear cluster formation, known as “cluster models,” are developed for the study of nuclear cluster states, as reviewed in Refs. [1–10]. On the other hand, many cluster states of light nuclei are of interest in astrophysics, such as the Hoyle state [11–13] and the CNO bicycle, which are important topics in both nuclear physics and astronomy. For example, the CNO bicycle provides a possible way for the synthesis of nuclides and explains the abundance of elements in the universe [14], where the ^{12}C and ^{13}C are both cornerstones in this process.

Theoretically, research has been conducted on the cluster states of $^{12-14}\text{C}$ isotopes, including the calculations based on the algebraic cluster model [15], semimicroscopic cluster models [16,17], and microscopic cluster models [18–22]. Phenomenologically, the rotational bands of cluster nuclei are well reproduced by the algebraic cluster model (ACM), focusing on the description of nuclear symmetry, such as the Z_2 symmetry for $2-\alpha$ systems, the D_{3h} symmetry for $3-\alpha$

*mengjiao.lyu@nuaa.edu.cn

†zren@tongji.edu.cn

systems, and the T_d symmetry for $4\text{-}\alpha$ systems [15,23,24]. Microscopic calculations of cluster states involve studies via the generator coordinate method (GCM) with Bloch-Brink wave functions [25], antisymmetrized molecular dynamics (AMD), and the Tohsaki-Horiuchi-Schuck-Röpke (THSR) wave functions, sometimes in conjunction with the molecular orbit (MO) model assumptions. In the GCM + Brink approach, the molecular orbits in the ground states of Be isotopes are studied in Refs. [20,26–28], where the intrinsic structure involves positioning α clusters and valence nucleons at generated coordinates, and the configuration mixing is calculated by solving the Hill-Wheeler equations. In AMD research, the nuclear cluster states for carbon, oxygen, and neon isotopes are described without the presumption of cluster formation [29–33], and some interesting structures, like the linear-chain and Hoyle-analog states for carbon isotopes, are discussed in Refs. [21,34–37].

The α condensate [1,2,5,7,10], proposed in Ref. [38], is a gaslike cluster structure that exists near the $N\text{-}\alpha$ threshold of nuclei where the center-of-mass motions of all α clusters are on the same s -wave orbit. Specifically, the Hoyle state of ^{12}C [11,12] is treated as an α condensate by the THSR wave function [38], where the exchange of nucleons between α clusters is microscopically described through full antisymmetrization. In subsequent works, THSR wave functions are extended to describe the compact α -cluster states in ^8Be , ^{12}C , ^{16}O , and ^{20}Ne as well [39–42]. Furthermore, THSR wave functions are also formulated for the non- $N\alpha$ nuclei such as ^{8-10}B , ^{9-10}Be , and ^{12}Be by introducing valence neutron(s) into the cluster structures [43–48]. It is shown that the square overlaps between the single THSR wave function and the GCM + Brink wave function exceed 90% in the well-developed α -cluster states of ^{12}C , ^{16}O , and ^{20}Ne , which provides a clear illustration for the α -cluster dynamics in these states through its extraordinarily simple analytical formulation [7,40,42,49–53]. Additionally, the π or σ molecular orbits in Be isotopes are described by the selection of THSR bases with proper symmetry [43–45]. In the THSR approach, intrinsic bases with the axial symmetry, commonly used in calculations of other cluster models, can be built straightforwardly using the concept of a “container” that we will introduce in Sec. II. Additionally, the intercluster correlation and the coupling between motions of clusters and valence neutrons are described by containers, which can lead the system to a certain rotational symmetry through the adjustment of them as well. These properties of the THSR wave function bring convenience and efficiency to the calculation and discussion of nuclear structure. For example, the THSR basis mixing can describe well the proton halo structure of ^8B in Ref. [48]. Furthermore, this approach explains the formation of NN -pairs in ^{10}B , ^{10}Be and ^{10}C in Ref. [47], and this work will discuss the $3\text{-}\alpha$ structure and its dissolution in $^{12-14}\text{C}$ isotopes.

For the $^{12-14}\text{C}$ isotopes, cluster structures are generally assumed for the excited states of ^{12}C above the $3\text{-}\alpha$ threshold [1], such as the Hoyle state, and are also suggested for those of ^{13}C and ^{14}C [13,54–57]. In many calculations the cluster structures are assumed for the ground state of ^{12}C as well [40,58]. However, the electromagnetic properties of ^{12}C [29,59–61] and also the strong binding of the ground

state, which lies 7.65 MeV below the Hoyle state, suggest a compact structure which is shell-like. In addition, the theoretical studies, using the Monte Carlo shell model (MCSM) [62] and antisymmetrized quasicluster model (AQCM) [29], suggest that the traditional clustering picture cannot fully describe the ground state of ^{12}C . Instead, both models propose a structure close to the quantum liquid in nuclear matter as the result of the cluster breaking effect [62]. Therefore, the cluster models [63–65] which rely on cluster assumptions should be expanded for a more accurate description of the properties of $^{12-14}\text{C}$ isotopes.

In cluster models the breaking of α clusters is treated partly by antisymmetrization between clusters but is not fully covered in the model space. Specifically, the paired excitation of nucleons within α clusters, which is favored by the spin-orbit terms in the nucleon-nucleon interaction, is not included in the cluster models. In principle, this issue can be addressed by using microscopic models with a full treatment of the nucleon degree of freedom, such as the AMD model. However, in such models it is difficult to trace the motions of correlated quasiparticles in the many-body system, such as α particles, while in cluster models the center-of-mass motions of α clusters are explicitly described by generator coordinates in the wave function. Thus, it is both challenging and interesting to develop a microscopic cluster model where both the formation and breaking effects of α clusters are fully treated in the wave function. In AQCM, the breaking or melting effect of α clusters is treated by exciting the nucleon-nucleon pairs with finite relative momentum inside the α clusters [19,29,61,66–68], including works for the ground states of ^{13}C and ^{14}C based on the GCM-Brink approach [18,69]. The nucleon-nucleon pairs with high relative momenta are also used to treat the two-particle–two-hole excitations induced by the tensor terms in the bare nucleon-nucleon interaction [70–72]. In works based on the GCM-Brink approach, the model space for cluster configurations is fully covered by the superposition of a large number of different basis states, and in some bases, the cluster-breaking (CB) effect is included. However, the motions of the broken clusters are still not fully revealed by the GCM wave function, as the structural information has to be extracted from the thousands of superposed basis states and only the terms with large weight in the state mixing are discussed. For instance, a regular triangular arrangement of the three α clusters is extracted from the Bloch-Brink basis states of ^{13}C [22] and ^{14}C [18]. For ^{12}C this is solved in Ref. [61], where the motions of broken α clusters are described explicitly by Gaussian weight functions (containers) in a THSR wave function incorporating CB pairs. In this work we introduce CB pairs into our extended THSR wave functions [43,44] to investigate the compact cluster states in the $^{12-14}\text{C}$ isotopes, especially focusing on the motions of broken α clusters.

This paper is organized as follows. In Sec. II we briefly formulate the THSR wave functions and the CB pairs for $^{12-14}\text{C}$ isotopes. We then explain the intrinsic configurations, where we consider two breaking modes for α clusters in CB-THSR wave functions and two coupling modes for valence neutrons in the ground states of ^{13}C and ^{14}C . In Sec. III the variational results which demonstrate the improvement of the

THSR approach after introducing the CB pairs in binding energy and matter rms radius are presented. The cluster structures described by different configurations are discussed, and the dominant components of their ground states are confirmed after the diagonalization of bases. Additionally, we optimize the interaction to reproduce the experimental spectra within both the THSR and CB-THSR frameworks. We also discuss the cluster breaking in a $3\text{-}\alpha$ system via the calculations of momentum distributions and form factors. Finally, Sec. IV presents the conclusions.

II. MICROSCOPIC APPROACH

A. Hamiltonian

The Hamiltonians of carbon isotopes used in this work are given as

$$\hat{H} = \sum_{i=1}^n k_i - k_{\text{c.m.}} + \sum_{i<j}^n V^N(\mathbf{r}_{ij}) + \sum_{i<j}^n V^C(\mathbf{r}_{ij}) + \sum_{i<j}^n V^{ls}(\mathbf{r}_{ij}), \quad (1)$$

where $\sum_{i=1}^n k_i$ and $k_{\text{c.m.}}$ are the kinetic energy term of nucleons and the center-of-mass term of the nucleus consisting of n nucleons, respectively. $V^N(\mathbf{r}_{ij})$ denotes the Volkov No. 2 interaction, which is an effective nucleon-nucleon interaction with the form

$$V^N(\mathbf{r}_{ij}) = \{V_1 e^{-\alpha_1 r_{ij}^2} - V_2 e^{-\alpha_2 r_{ij}^2}\} \times \{W - M \hat{P}_\sigma \hat{P}_\tau + B \hat{P}_\sigma - H \hat{P}_\tau\}. \quad (2)$$

Here, $V_1 = -60.650$ MeV, $V_2 = 61.140$ MeV, $\alpha_1 = 0.980$ fm $^{-2}$, $\alpha_2 = 0.309$ fm $^{-2}$, and the exchange parameters are $W = 0.4$, $M = 0.6$, and $B = H = 0.125$. All of these parameters are determined from the $\alpha + n$ and $\alpha + \alpha$ scattering phase shifts and the binding energy of the deuteron [73]. $V^C(\mathbf{r}_{ij})$ is the Coulomb interaction. The G3RS force is used for the spin-orbit interaction $V^{ls}(\mathbf{r}_{ij})$ with the form of

$$V^{ls}(\mathbf{r}_{ij}) = u_{ls} \{e^{-\alpha_1 r_{ij}^2} - e^{-\alpha_2 r_{ij}^2}\} \mathbf{L} \cdot \mathbf{S} \hat{P}_{31}, \quad (3)$$

where $u_{ls} = 2000$ MeV, $\alpha_1 = 5.00$ fm $^{-2}$, and $\alpha_2 = 2.778$ fm $^{-2}$ [27].

B. THSR wave function

In THSR approach, the wave function for ^{12}C can be written as

$$|\Phi_{^{12}\text{C}}^{\text{THSR}}\rangle = (C_\alpha^\dagger)^3 |\text{vac}\rangle, \quad (4)$$

where C_α^\dagger is the creation operator of an α cluster:

$$C_\alpha^\dagger = \int d\mathbf{R} \mathcal{G}_\alpha(\mathbf{R}) \int d^3\mathbf{r}_1 \cdots d^3\mathbf{r}_4 \times \phi(\mathbf{r}_1 - \mathbf{R}) a_{\sigma_1, \tau_1}^\dagger(\mathbf{r}_1) \cdots \phi(\mathbf{r}_4 - \mathbf{R}) a_{\sigma_4, \tau_4}^\dagger(\mathbf{r}_4). \quad (5)$$

In the equation the spatial part of a single particle is defined as

$$\phi(\mathbf{r} - \mathbf{R}) \propto \exp\left\{-\frac{(\mathbf{r} - \mathbf{R})^2}{2b^2}\right\}, \quad (6)$$

where “ b ” is fixed to be 1.46 fm for all nucleons [44], and $a_{\sigma, \tau}^\dagger$ is the creation operator for a nucleon with spin σ and isospin τ . The “Gaussian container” [42], proposed to describe α -condensate states [38], is adopted to confine the motions of α clusters and defined by the function

$$\mathcal{G}_\alpha(\mathbf{R}) = \exp\left\{-\frac{R_x^2 + R_y^2}{\beta_{\alpha, xy}^2} - \frac{R_z^2}{\beta_{\alpha, z}^2}\right\}, \quad (7)$$

where $\beta_{\alpha, xy}$ and $\beta_{\alpha, z}$ are the parameters to be optimized by variational calculations.

For ^{13}C and ^{14}C isotopes, THSR wave functions are formulated with the additional creation operators for valence nucleons, such as

$$|\Phi_{^{13}\text{C}}^{\text{THSR}}\rangle = (C_\alpha^\dagger)^3 (c_n^\dagger) |\text{vac}\rangle \quad (8)$$

and

$$|\Phi_{^{14}\text{C}}^{\text{THSR}}\rangle = (C_\alpha^\dagger)^3 (c_n^\dagger)^2 |\text{vac}\rangle, \quad (9)$$

respectively. The creation operator c_n^\dagger is formulated as

$$c_n^\dagger = \int d\mathbf{R} \mathcal{G}_n(\mathbf{R}) \int d^3\mathbf{r} \phi(\mathbf{r} - \mathbf{R}) a_{\sigma, \tau}^\dagger(\mathbf{r}). \quad (10)$$

The term $\mathcal{G}_n(\mathbf{R})$ is the “container” for valence neutrons, which is modulated by a phase factor [43] or a spherical harmonic function [48] to reproduce the negative parity of π orbit. Here, we take the one formulated in Ref. [48] for the efficiency in numerical calculation, which is given as

$$\mathcal{G}_n(\mathbf{R}) = \exp\left\{-\frac{R_x^2 + R_y^2}{\beta_{n, xy}^2} - \frac{R_z^2}{\beta_{n, z}^2}\right\} Y_{lm}(\mathbf{R}_\Omega), \quad (11)$$

where \mathbf{R}_Ω is the angular part of the generator coordinate \mathbf{R} , and the parameter m is the magnetic quantum number for the valence neutron. We noted that the $\mathcal{G}_n(\mathbf{R})$ will reduce to a Gaussian packet when l and m are both zero. For more details please refer to Ref. [43].

C. Angular momentum coupling and projection

Using Eqs. (4), (8), and (9), we can formulate the THSR basis wave functions for $^{12-14}\text{C}$ isotopes. For ^{12}C the THSR wave function is formulated with good magnetic quantum number $m = 0$. For ^{13}C and ^{14}C , treated as “ $3\text{-}\alpha + (2)n$ ” systems, the angular momenta of α clusters are coupled with those of valence nucleons. As shown in Table I, we consider two THSR basis functions for both ^{13}C and ^{14}C , with different angular momentum couplings between α clusters and valence neutrons, denoted as “Coupling Mode 1” (CM. 1) and “Coupling Mode 2” (CM. 2), respectively.

To restore the total rotational symmetry, THSR basis wave functions are projected by the corresponding angular

TABLE I. Two angular momentum coupling modes for ^{13}C and ^{14}C . S_n denotes the spin of each valence neutron. m represents the quantum number of z component on orbital angular momentum for each valence neutron. The spherical harmonic in the container of each valence neutron is set to be $Y_{lm}(\mathbf{R}_\Omega)$.

Coupling mode (CM.)	$^{13}\text{C}(1/2^-)$		$^{14}\text{C}(0^+)$			
1	$S_n = \uparrow\rangle_z$	$m = 0$	$S_{n,1} = \uparrow\rangle_z$	$m_{n,1} = 0$	$S_{n,2} = \downarrow\rangle_z$	$m_{n,2} = 0$
2	$S_n = \uparrow\rangle_z$	$m = -1$	$S_{n,1} = \uparrow\rangle_z$	$m_{n,1} = -1$	$S_{n,2} = \downarrow\rangle_z$	$m_{n,2} = 1$

momentum projection operators [74], given as

$$\hat{P}_{M,K}^J = \frac{2J+1}{8\pi^2} \int_0^{2\pi} d\phi \int_0^\pi d\theta \sin(\theta) \int_0^{2\pi} d\gamma \quad (12)$$

$$\times D_{M,K}^{J*}(\phi, \theta, \gamma) \hat{R}(\phi, \theta, \gamma),$$

where $D_{M,K}^J(\phi, \theta, \gamma)$ is the Wigner's D function of the three Euler angles ϕ , θ , and γ . The projected basis wave function is thus

$$\Psi_M^J = \hat{P}_{M,K}^J \Psi^{\text{THSR}}. \quad (13)$$

D. CB-THSR wave function

In pure cluster models, four nucleons share the same generator coordinate \mathbf{R} in an α cluster, with zero relative momenta. To describe the cluster breaking, we introduce the nucleon-nucleon pairs into the THSR approach. In each pair two nucleons are selected from the same α cluster with opposite spin orientations, and they are excited relative to each other in momentum space. In this work we refer to these pairs as ‘‘CB pairs.’’ A CB pair is mathematically represented by adding opposite imaginary components to the generator coordinates of the nucleons [75]:

$$\begin{aligned} \mathbf{R}_i &\rightarrow \mathbf{R}_i + i\Lambda \mathbf{e} \\ \mathbf{R}_j &\rightarrow \mathbf{R}_j - i\Lambda \mathbf{e}. \end{aligned} \quad (14)$$

Here, \mathbf{R}_i and \mathbf{R}_j are the generator coordinates of two nucleons in the CB pair, Λ is the amplitude of cluster breaking excitation, and the unit vector \mathbf{e} denotes the direction of $\mathbf{s} \times \text{Re}[\mathbf{R}]$, where \mathbf{s} is the spin of the nucleon. In these CB pairs, nucleons are excited with a mean momentum as

$$\frac{\langle \phi | \mathbf{p} | \phi \rangle}{\langle \phi | \phi \rangle} = \frac{\hbar}{b^2} \text{Im}(\mathbf{R}) = \frac{\hbar}{b^2} \Lambda \mathbf{e}. \quad (15)$$

With the definition of unit vector \mathbf{e} , the relative momentum is oriented perpendicular to the spins of two nucleons within a CB pair. Here we introduce the CB pairs with opposite spins in two different cases: one with spins confined on the xy plane and the other one along the z axis, which correspond to two different modes for the relative momenta along the z direction and on the xy plane, respectively, as listed in Table II. Both breaking modes contribute to the cluster breaking effect within the $3\text{-}\alpha$ core, and we denote them as ‘‘breaking mode I (BM. I)’’ and ‘‘breaking mode II (BM. II).’’ Moreover, we note that BM. I is highly possible to have equilateral triangular symmetry when the THSR wave function becomes oblate and compact. It is because the three α clusters tend to form an equilateral triangle located on the xy plane in such a configuration, with the spins in each CB pair being perpendicular to the generator coordinates of α clusters.

III. RESULTS AND DISCUSSION

A. Results of the original THSR wave function

We first investigate $^{12-14}\text{C}$ isotopes by using the original THSR basis wave functions. The optimal β parameters and corresponding minimum energies are obtained via variational calculations, as listed in Table III. Here the optimal energy of ^{12}C is located at $\beta_{xy} = \beta_z = 1.4$ fm, which is consistent with Ref. [40] and indicates the spherical symmetry for the $3\text{-}\alpha$ cluster state.

For ^{13}C and ^{14}C , with CM. 1 we obtain $\beta_{xy} = 1.6$ fm and $\beta_z = 0.2$ fm for both nuclei, which show the oblate deformation of the $3\text{-}\alpha$ cores. With CM. 2 we find $\beta_{xy} = 1.0$ fm, $\beta_z = 1.4$ fm for ^{13}C , and $\beta_{xy} = 1.4$ fm, $\beta_z = 1.6$ fm for ^{14}C , which indicate the prolate structures for the $3\text{-}\alpha$ cores. On the other hand, the two THSR basis functions respectively describe the motions of valence neutrons as dumbbell-like π orbits in CM. 1 and ringlike π orbits in CM. 2. Here we observe two distinct core-valence couplings between the $3\text{-}\alpha$ core and the valence neutrons. We conclude that the motions of α clusters are constrained by those of the valence neutrons due to these couplings, which is the reason for the strong deformation of the $3\text{-}\alpha$ cores in $^{13-14}\text{C}$ isotopes.

In real nuclei there is configuration mixing between these two different THSR basis functions in the ground states of ^{13}C and ^{14}C . In Table III it is found that the configuration with CM. 1 shows lower energy in both ^{13}C and ^{14}C , which indicates a larger contribution in the mixing. This is also shown in Fig. 3. Indeed, after superposing two THSR basis functions, the ground-state energies are obtained for $^{13-14}\text{C}$ isotopes, and the values are almost equal to those produced by configuration 1 only.

Using the original THSR wave functions, we find the deformation of the α clusters and their couplings with the valence neutrons. However, as shown in Table III, the binding energies of carbon isotopes are significantly underestimated. This is expected because the significant cluster breaking effect is not optimized in the original THSR, which is essential for the compact structures of $^{12-14}\text{C}$ isotopes.

TABLE II. Two breaking modes for CB pairs within α clusters. The different spin orientations of paired nucleons and their corresponding orientations of relative momentum are shown.

Breaking mode (BM.)	Orientations of nucleon spins within α clusters	Orientation of relative momentum
I	xy plane	z axis
II	z axis	xy plane

TABLE III. The energies of $^{12-14}\text{C}$ isotopes obtained by the original THSR basis wave functions. Two intrinsic configurations with distinct angular momentum coupling modes are adopted for ^{13}C and ^{14}C . The β parameters and energies are obtained after the angular momentum projection and variational optimization.

		THSR				Energy (MeV)	Exp (MeV)
	Configurations	$\beta_{xy}(\text{fm})$	$\beta_z(\text{fm})$	$\beta_{n,xy}(\text{fm})$	$\beta_{n,z}(\text{fm})$		
^{12}C	–	1.4	1.4	–	–	–85.9	–92.16
^{13}C	CM. 1	1.6	0.2	3.8	1.6	–91.6	–97.11
	CM. 2	0.6	1.0	1.0	4.6	–89.1	
^{14}C	CM. 1	1.2	0.2	3.2	2.0	–99.6	–105.3
	CM. 2	0.6	0.8	1.0	3.6	–98.5	

B. Results of the CB-THSR wave function

For compact cluster states, we introduce the CB pairs into the THSR wave functions to allow a further α -cluster breaking as compared to antisymmetrization. This will also produce a mixing state between the well-developed cluster state and the shell-like state. Using this approach, we calculate again the ground states of $^{12-14}\text{C}$ isotopes with two breaking modes of α clusters, and the results are listed in Table IV. Compared to the original THSR results shown in Table III, improved binding energies, which are closer to the experimental data, are obtained for $^{12-14}\text{C}$ isotopes. For ^{12}C we obtain $\beta_{xy} = 0.4$, $\beta_z = 0.2$ fm and $\beta_{xy} = 0.4$, $\beta_z = 0.8$ fm in the wave functions with BM. I and BM. II, respectively, which are now deformed in the CB-THSR calculations. For ^{13}C and ^{14}C , the core-valence couplings between the 3- α cores and the valence neutrons, as shown in the density plots in Fig. 1, are similar to those of the original THSR description with “BM. I + CM. 1” and “BM. II + CM. 2”, except that the 3- α cores are much more compact in the CB-THSR, as shown by the small parameters β_{xy} and β_z . However, the other two configurations “BM. I + CM. 2” and “BM. II + CM. 2” provide new descriptions, where “BM. I + CM. 2” results in the most compact structure, which is shell-like, and “BM. II + CM. 1” yields an oblate clustering

structure. For ^{13}C the configurations “BM. I + CM. 1” and “BM. I + CM. 2” produce identical energy values of –100.2 MeV, showing that these two configurations are very similar to each other. This is further confirmed by a large overlap of 0.97 between these two configurations after angular momentum projection. For ^{14}C the overlap reduces to 0.90, which indicates discrepancy between the two configurations. The relatively lower energy value of –108.6 produced by “BM. I + CM. 2” suggests its dominance in the ground state, as shown in Fig. 2. We note that valence neutrons have relatively larger β parameters compared to those of α clusters, as shown in Table IV, indicating their extended motion around the 3- α cores. The root-mean-squared radii calculated for valence neutrons are 2.82 and 2.63 fm for the configurations “BM. I + CM. 2” and “BM. II + CM. 2” in ^{13}C , respectively. For ^{14}C both configurations yield an rms radius of 2.83 fm for valence neutrons.

Finally, we superpose all the THSR basis functions for $^{12-14}\text{C}$ isotopes, and also compare them with the results of other theoretical works and the experimental data as well. The results are shown in Fig. 3. It is clearly seen that the binding energies are significantly improved with the cluster breaking effect introduced for $^{12-14}\text{C}$ isotopes, as compared to the original THSR results. However, they are now overbound when

TABLE IV. The energies of $^{12-14}\text{C}$ isotopes calculated by the CB-THSR basis wave functions. Two configurations with distinct breaking modes of α -clusters are adopted for ^{12}C , and four configurations in which two breaking modes of α -clusters combine with two angular momentum coupling modes are adopted for ^{13}C and ^{14}C . The β parameters and energies are obtained after the angular momentum projection and variational optimization.

		CB-THSR						Energy (MeV)	Exp (MeV)
	Configurations	$\beta_{xy}(\text{fm})$	$\beta_z(\text{fm})$	$\beta_{n,xy}(\text{fm})$	$\beta_{n,z}(\text{fm})$	$\Lambda(\text{fm})$			
^{12}C	BM. I	0.4	0.2	–	–	0.2	–93.7	–92.16	
	BM. II	0.4	0.8	–	–	0.2	–91.0		
^{13}C	BM. I + CM. 1	0.6	0.2	1.6	2.0	0.3	–100.2	–97.11	
	BM. I + CM. 2	0.2	0.2	1.2	6.4	0.5	–100.2		
	BM. II + CM. 1	1.6	0.2	3.8	1.6	0.0	–91.6		
	BM. II + CM. 2	0.2	0.6	0.6	5.8	0.2	–98.3		
^{14}C	BM. I + CM. 1	0.6	0.2	3.0	2.4	0.3	–107.6	–105.3	
	BM. I + CM. 2	0.2	0.2	1.2	5.6	0.5	–108.6		
	BM. II + CM. 1	1.2	0.2	3.2	2.0	0.0	–99.6		
	BM. II + CM. 2	0.4	0.6	1.2	5.6	0.3	–108.1		

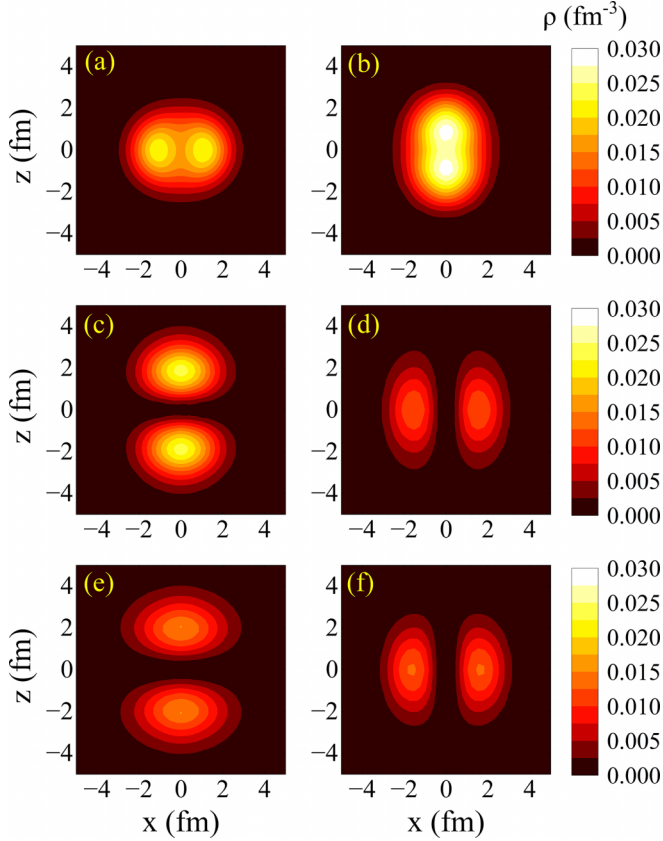


FIG. 1. The intrinsic density distributions of nucleons in $^{12-14}\text{C}$ isotopes in the $y = 0$ cross section. Panels (a) and (b) are the density plots for nucleons in ^{12}C with BM. I and BM. II, respectively, given by the CB-THSR basis functions. Panels (c) and (d) are the density plots for the valence neutron in ^{13}C described by CB-THSR with CM. 1 and CM. 2, respectively. Panels (e) and (f) are the density plots for valence neutrons in ^{14}C described by CB-THSR with CM. 1 and CM. 2, respectively.

comparing to the experimental values. We thus further adopt a weakened $M = 0.62$ nucleon-nucleon attraction in Volkov force and $u_{ls} = 2250$ MeV strength of spin-orbit interaction in the CB-THSR calculation for better consistency with the experimental data. Additionally, the theoretical results presented in other works using the same interaction $M = 0.6$ and $u_{ls} = 2000$ MeV are also shown in Fig. 3. Here we note that the result adopted from Ref. [19] is for the microscopic calculation of ^{12}C with the breaking effect included. It is thus reasonable that the result is consistent with ours. The other two values adopted from Refs. [22] and [18] are calculated without including the cluster breaking effect for ^{13}C and ^{14}C , respectively. It is thus reasonable that the binding energies are much smaller in magnitude compared to the CB-THSR ones. These comparisons show the indispensable role of the cluster breaking effect in understanding the ground states of $^{12-14}\text{C}$ isotopes.

C. Optimization

To obtain more accurate ground-state spectra for $^{12-14}\text{C}$ isotopes, we further optimize the effective nucleon-nucleon

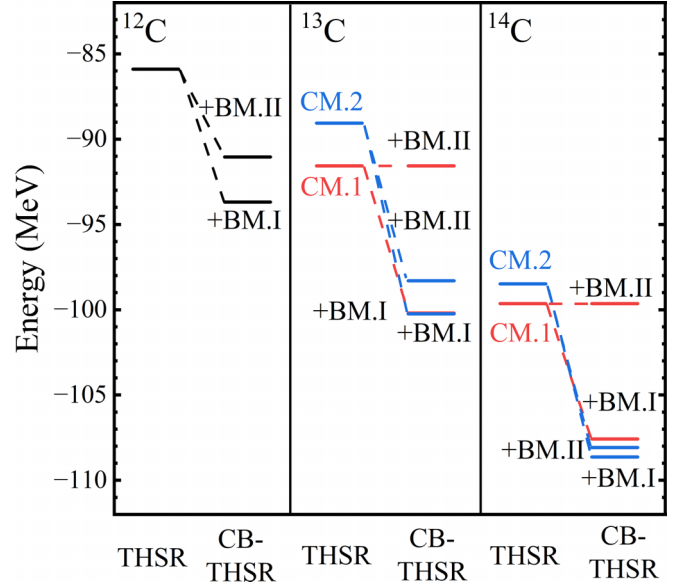


FIG. 2. Energies of $^{12-14}\text{C}$ isotopes obtained by using the original THSR and CB-THSR basis functions with different configurations. “CM.” denotes the angular momentum coupling mode. “+BM.” represents the configuration considering the breaking mode based on the corresponding coupling mode.

interaction through adjusting M and u_{ls} , where M is the parameter in Volkov force, and u_{ls} is the strength of spin-orbit interaction. Figure 4 exhibits the results of THSR and CB-THSR in panels (a)–(c) and (d)–(f), respectively, with the energy error defined as $\Delta E = E_{\text{theory}} - E_{\text{exp}}$. It is found that the CB-THSR framework achieves better consistency in

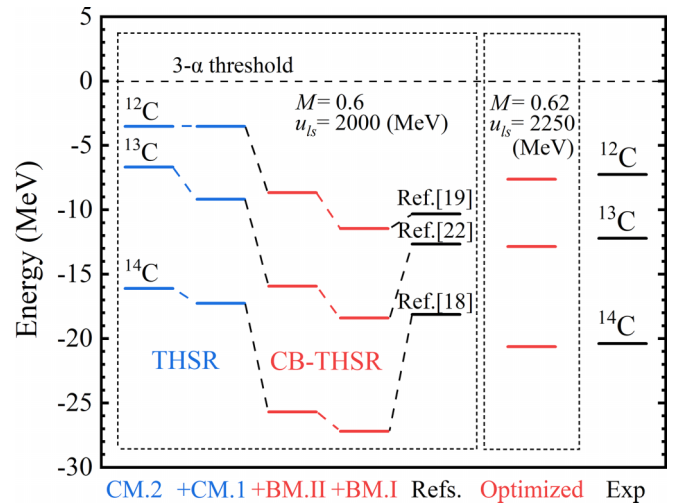


FIG. 3. The energies after superposition, relative to the 3α threshold. “CM.” and “BM.” denote the angular momentum coupling mode and the breaking mode of α clusters, respectively. M is the parameter in nucleon-nucleon interaction, and u_{ls} is the coupling strength in spin-orbit interaction. The energies of $^{12-14}\text{C}$ isotopes in the “Refs.” column are the results calculated with the same Hamiltonian and $M = 0.6$, $u_{ls} = 2000$ MeV, adopted from corresponding references.

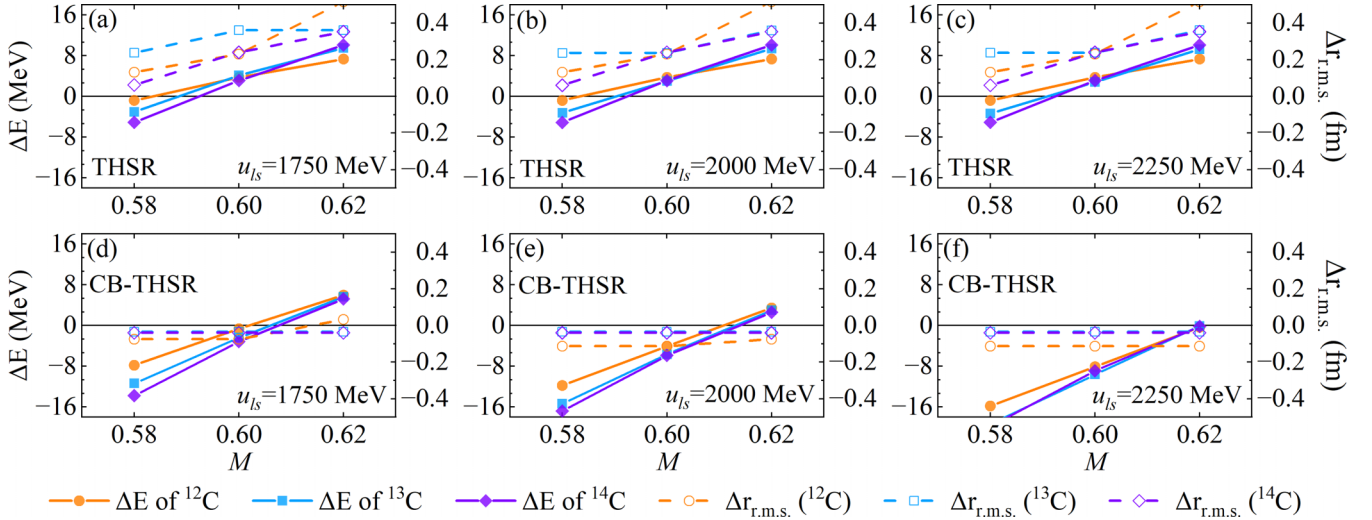


FIG. 4. The ground-state energies and rms radii calculated by using THSR and CB-THSR wave functions with different M in nucleon-nucleon interaction and u_{ls} in spin-orbit interaction. “ ΔE ” denotes the energy error, defined as $E_{\text{theory}} - E_{\text{exp}}$. “ $\Delta r_{\text{r.m.s.}}$ ” denotes the rms radius error, defined as $r_{\text{r.m.s.}}(\text{theory}) - r_{\text{r.m.s.}}(\text{exp})$.

binding energies compared to the original THSR. On the other hand, a smaller value is obtained for the parameter M after energy optimization in THSR as compared to the initial one, which corresponds to an enhanced nucleon-nucleon attraction. In contrast, a larger M is obtained in CB-THSR, suggesting a reduction of nucleon-nucleon attraction. Additionally, it is found that the spin-orbit (LS) coupling plays a significant role in the optimization for CB-THSR, but is not sensitive in THSR calculations.

To summarize, with the optimized weaker nucleon-nucleon attraction and the adjusted spin-orbit interaction, CB-THSR can produce a more accurate ground-state spectra for $^{12-14}\text{C}$ isotopes compared to THSR.

D. Matter rms radius

To further illustrate the α -cluster structures in $^{12-14}\text{C}$ isotopes, we calculate their matter root-mean-square radii, as shown in Table V, with $M = 0.6$ in nucleon-nucleon interaction and $u_{ls} = 2000$ MeV in spin-orbit interaction. Additionally, the rms radii with adjusted M and u_{ls} are also calculated, and the errors, defined as $\Delta R = R_{\text{theory}} - R_{\text{exp}}$, are exhibited in Fig. 4 as well. As compared to the experimental data, the original THSR wave functions produce

much larger rms radii, corresponding to well-developed α -cluster states for $^{12-14}\text{C}$ isotopes. After the introduction of CB pairs and variational calculations, the structures shrink into compact ones with smaller rms radii, which are now more consistent with the experimental data. Moreover, the rms radii are not sensitive to the variation of u_{ls} in CB-THSR calculations, which shows the structural saturation for the ground states of $^{12-14}\text{C}$ isotopes.

E. Momentum distribution and form factor

In the CB-THSR wave function, cluster breaking can be induced by both antisymmetrization and CB pairs. It is of interest to find which one makes a major contribution to the cluster breaking in the compact α -cluster states of $^{12-14}\text{C}$ isotopes. In Ref. [77], the nucleon momentum distribution, which could be measured with high precision using e, e' scattering [78], is discussed for beryllium isotopes, and it is found that the real distribution of the nuclei deviates from the Gaussian form when the α clusters are broken due to antisymmetrization. In this work we use a similar strategy to discuss the cluster breaking effects in the 3- α system of ^{12}C with the calculations of momentum distributions. As we noted in previous sections, original THSR wave functions involve cluster breaking only

TABLE V. The matter rms radii of $^{12-14}\text{C}$ isotopes calculated by using original THSR and CB-THSR wave functions. Two sets of parameters where $M = 0.6$, $u_{ls} = 2000$ MeV and $M = 0.62$, $u_{ls} = 2250$ MeV for nucleon-nucleon interaction and spin-orbit interaction are adopted. The experimental data are taken from Ref. [76].

	Original THSR ($M = 0.6$, $u_{ls} = 2000$ MeV)	CB-THSR ($M = 0.6$, $u_{ls} = 2000$ MeV)	CB-THSR ($M = 0.62$, $u_{ls} = 2250$ MeV)	Exp
^{12}C	2.58	2.24	2.24	2.35(2)
^{13}C	2.52	2.25	2.25	2.28(4)
^{14}C	2.57	2.29	2.29	2.33(7)

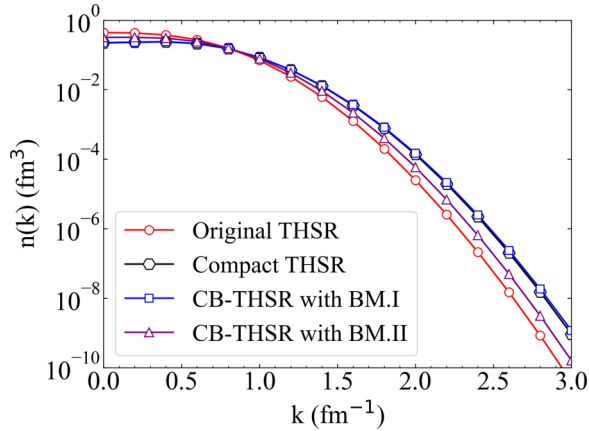


FIG. 5. Momentum distributions of ^{12}C calculated with four configurations simulating different $3\text{-}\alpha$ cores in $^{12-14}\text{C}$ isotopes. “Original THSR” denotes the result of original THSR wave function with $\beta_{xy} = \beta_z = 1.4$ fm, which corresponds to a well-developed cluster state in ^{12}C . “Compact THSR” denotes the result of THSR wave functions with $\beta_{xy} = 0.8$ fm and $\beta_z = 0.2$ fm, to simulate the compact $3\text{-}\alpha$ -cluster cores in ^{13}C and ^{14}C . “CB-THSR with BM. I” and “CB-THSR with BM. II” show the results from CB-THSR wave functions, with the corresponding optimal parameters when $M = 0.62$ in nucleon-nucleon interaction and $u_{ls} = 2000$ MeV in spin-orbit interaction to simulate the $3\text{-}\alpha$ cores when CB pairs are introduced.

through antisymmetrization, and CB-THSR wave functions allow cluster breaking induced by both antisymmetrization and CB pairs. In Fig. 5 the red curve with circles (labeled “Original THSR”) denotes the result of the original THSR wave function with spherical set $\beta_{xy} = \beta_z = 1.4$ fm, which corresponds to a well-developed cluster state in ^{12}C . The gray curve with hexagons (labeled “Compact THSR”) denotes the result of the original THSR wave function with $\beta_{xy} = 0.8$ fm and $\beta_z = 0.2$ fm, simulating the compact $3\text{-}\alpha$ cores in $^{13-14}\text{C}$ isotopes. The blue curve with squares (labeled “CB-THSR with BM. I”) shows the result from CB-THSR wave function with BM. I and also $\beta_{xy} = 0.8$ fm and $\beta_z = 0.2$ fm, to investigate the further broken $3\text{-}\alpha$ cores when CB pairs are introduced. This configuration corresponds to the structure with the most accurate rms radii, obtained from the variational calculation using $M = 0.62$ in the nucleon-nucleon potential. As for CB-THSR with BM. II, the result is represented by the purple curve with triangles (labeled “CB-THSR with BM. II”) with $\beta_{xy} = 1.2$ fm and $\beta_z = 1.6$ fm, also obtained from the variational calculation.

In Fig. 5 it is clearly shown that the “Compact THSR,” “CB-THSR with BM. I,” and “CB-THSR with BM. II” exhibit smaller low-momentum components and a larger tail in the high-momentum region compared to the “Original THSR.” This indicates that the α clusters are significantly broken due to the strong antisymmetrization in their compact $3\text{-}\alpha$ cores. Although both antisymmetrization and CB pairs can induce cluster breaking effects, this comparison demonstrates that antisymmetrization dominates the cluster breaking effect within a compact $3\text{-}\alpha$ system. For a more detailed discussion of the effects from antisymmetrization, please refer to Ref. [77]. In

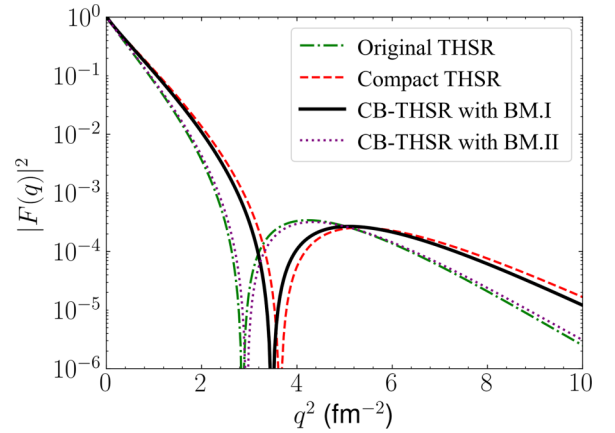


FIG. 6. Form factors of ^{12}C calculated with four configurations on a logarithmic scale. “Original THSR” denotes the result of original THSR wave function with $\beta_{xy} = \beta_z = 1.4$ fm. “Compact THSR” denotes the result of THSR wave function, with $\beta_{xy} = 0.8$ fm and $\beta_z = 0.2$ fm. “CB-THSR with BM. I” and “CB-THSR with BM. II” show the results from corresponding CB-THSR wave functions, with $\beta_{xy} = 0.8$ fm, $\beta_z = 0.2$ fm and $\beta_{xy} = 1.2$ fm and $\beta_z = 1.6$ fm, respectively.

addition, we notice that the momentum distributions produced by “Compact THSR” and “CB-THSR with BM. I” are very similar to each other, which indicates a comparable level of cluster breaking excitations for nucleons. However, the former one is energetically unfavorable while the latter significantly enhances the binding energy of the ground state. This drastic difference indicates that the CB-THSR provides a better description for the physical breaking of α clusters in the ground state of ^{12}C with combining antisymmetrization and CB pairs. Theoretically speaking, the antisymmetrization between overlapping clusters describes their exchange of particles, while the CB pairs focus on the paired excitation. This comparison suggests that we should consider both particle exchange and paired excitations when discussing compact cluster states.

We also compare the CB-THSR with the original THSR wave functions via the calculations of form factors, which are defined as the Fourier transform of charge density distributions. The results are shown on a logarithmic scale in Fig. 6 and on a linear scale in Fig. 7. We note that the β values in wave functions are adopted as the optimized values corresponding to the interaction parameters $M = 0.62$ and $u_{ls} = 1750$ MeV, which provides the best description for ^{12}C as shown in Fig. 4. In Fig. 6 the black solid curve denotes the form factor of “CB-THSR with BM. I,” which is the dominant component in the ground-state wave function. The red-dashed curve represents the form factor of “Compact THSR,” which is similar to that of “CB-THSR with BM. I.” This indicates that the two configurations have similar radii and cluster breaking. For comparison, the form factor of “Original THSR” is shown as the green dash-dotted curve, while the “CB-THSR with BM. II” is presented as the purple dotted curve. These two curves are also similar but deviate from the solid curve, indicating a lesser degree of cluster breaking.

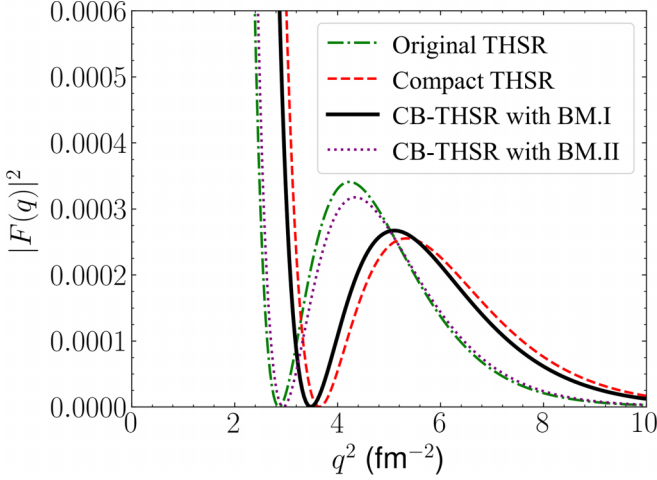


FIG. 7. Form factors of ^{12}C calculated with four configurations on a linear scale. “Original THSR” denotes the result of original THSR wave functions with $\beta_{xy} = \beta_z = 1.4$ fm. “Compact THSR” denotes the result of THSR wave function, with $\beta_{xy} = 0.8$ fm and $\beta_z = 0.2$ fm. “CB-THSR with BM. I” and “CB-THSR with BM. II” show the results from corresponding CB-THSR wave functions, with $\beta_{xy} = 0.8$ fm, $\beta_z = 0.2$ fm and $\beta_{xy} = 1.2$ fm and $\beta_z = 1.6$ fm, respectively.

IV. CONCLUSION

We investigated the ground states of $^{12-14}\text{C}$ isotopes using both THSR and CB-THSR wave functions. For describing the intrinsic cluster structures of compact carbon isotopes, the THSR wave functions were formulated for the different modes of cluster and valence neutron motions, which we named “Coupling Modes (CM.)” For ^{12}C a spherical structure was produced, consistent with those in previous works. ^{13}C and ^{14}C were each described by a superposition of two configurations, including one with dumbbell-like molecular orbits of valence neutrons coupled with an oblate $3-\alpha$ core, and another with a prolate $3-\alpha$ core surrounded by ring-like distributions of valence neutrons. It was found that the couplings of motions between clusters and valence neutrons determine the cluster structure in each configuration, as revealed by variational calculations. However, the calculated binding energies appear to be underestimated, and the matter rms radii are significantly larger than the experimental values. CB pairs were further introduced into THSR wave functions to formulate “CB-THSR” wave functions. Different orientations of spin within CB pairs led to different modes of paired excitation, which we named “Breaking Modes (BM.)” After introducing the CB pairs, the CB-THSR wave functions produced more compact structures for $^{12-14}\text{C}$ isotopes, and energy results showed better consistency with the experimental values. In addition, the effects of CB pairs were found to be dependent on the different configurations. The nucleon-nucleon and spin-orbit interaction dependencies have also been discussed by comparing the results calculated using various parameters. Compared to THSR, CB-THSR suggests a weaker attraction in the nucleon-nucleon interaction.

The spatial extension of cluster structures has been further discussed by the calculations of rms radii, where CB-THSR provides systematically better results as compared to the original THSR wave functions. Finally, we investigated the cluster breaking effects in $^{12-14}\text{C}$ isotopes by comparing the nucleon momentum distributions and the charge form factors of strongly antisymmetrized cluster states, with and without the introduction of CB pairs. It was found that both the compact THSR and the CB-THSR with BM. I produce a comparable level of α -cluster breaking, but only the latter significantly enhances the binding energy of the ground state, showing that the CB-THSR describes better the physical breaking of α clusters in the ground state of ^{12}C . This comparison suggests that we should consider both particle exchange and paired excitation when discussing compact cluster states, thereby offering a more complete description of cluster breaking effects in theoretical models.

ACKNOWLEDGMENTS

We are immensely grateful and deeply miss Prof. Peter Schuck’s collaborative research and discussions on cluster physics over the years. This work is supported by the National Natural Science Foundation of China (Grants No. 12035011, No. 11975167, and No. 12105141), by Jiangsu Provincial Natural Science Foundation (Grant No. BK20210277), by the National Key R&D Program of China (Contract No. 2023YFA1606503), and the 2021 Jiangsu Shuangchuang (Mass Innovation and Entrepreneurship) Talent Program (Grant No. JSSCBS20210169).

APPENDIX

1. Momentum distribution

In Brink-THSR framework, the momentum distribution of the N -body system is defined as

$$n(\mathbf{a}) = \frac{\langle \Phi | \sum_{i=1}^N \hat{n}_i(\mathbf{a}) | \Phi \rangle}{\langle \Phi | \Phi \rangle}, \quad (\text{A1})$$

where $n(\mathbf{a})$ denotes the amplitude at momentum \mathbf{a} . The subscript i is for the number of nucleons, and the operator $\hat{n}_i(\mathbf{a})$ is defined as $\delta(\mathbf{k}_i - \mathbf{a})$, where \mathbf{k}_i is the momentum of the i th nucleon. $n(\mathbf{a})$ is now written as

$$n(\mathbf{a}) = \frac{\langle \Phi | \sum_{i=1}^N \delta(\mathbf{k}_i - \mathbf{a}) | \Phi \rangle}{\langle \Phi | \Phi \rangle}. \quad (\text{A2})$$

In the Brink-THSR wave functions, the total wave function incorporates the spurious center-of-mass motion, which can be separated into intrinsic wave function and center-of-mass wave function,

$$\Phi^{\text{Tot}} = \Phi^{\text{Int}} \Phi^{\text{c.m.}},$$

where the superscript “Tot” denotes total wave function, “Int” denotes intrinsic wave function, and “c.m.” denotes center-of-mass motion. To find the momentum distribution without center of mass, we introduce notation for momentum \mathbf{b} in the intrinsic frame, which is related to the momentum \mathbf{k} in total

wave function as

$$\mathbf{k} = \mathbf{b} + \mathbf{k}_G/N,$$

where \mathbf{k}_G denotes the momentum of center of mass. After the Fourier transform, the intrinsic momentum distribution is written as

$$n^{\text{Int}}(\mathbf{a}) = \left(\frac{1}{2\pi}\right)^3 \sum_{i=1}^N \int d^3\mathbf{r} e^{-i\mathbf{a}\cdot\mathbf{r}} \frac{\langle \Phi^{\text{Int}} | e^{i\mathbf{b}\cdot\mathbf{r}} | \Phi^{\text{Int}} \rangle}{\langle \Phi^{\text{Int}} | \Phi^{\text{Int}} \rangle}. \quad (\text{A3})$$

The momentum distribution with center-of-mass motion included for total wave function is written as

$$\begin{aligned} n^{\text{Tot}}(\mathbf{a}) &= \left(\frac{1}{2\pi}\right)^3 \sum_{i=1}^N \int d^3\mathbf{r} e^{-i\mathbf{a}\cdot\mathbf{r}} \frac{\langle \Phi^{\text{Tot}} | e^{i\mathbf{k}_i\cdot\mathbf{r}} | \Phi^{\text{Tot}} \rangle}{\langle \Phi^{\text{Tot}} | \Phi^{\text{Tot}} \rangle} \\ &= \left(\frac{1}{2\pi}\right)^3 \sum_{i=1}^N \int d^3\mathbf{r} e^{-i\mathbf{a}\cdot\mathbf{r}} \\ &\quad \times \frac{\langle \Phi^{\text{Int}} | e^{i\mathbf{k}_i\cdot\mathbf{r}} | \Phi^{\text{Int}} \rangle}{\langle \Phi^{\text{Int}} | \Phi^{\text{Int}} \rangle} \frac{\langle \Phi^{\text{c.m.}} | e^{i\mathbf{k}_G\cdot\mathbf{r}/N} | \Phi^{\text{c.m.}} \rangle}{\langle \Phi^{\text{c.m.}} | \Phi^{\text{c.m.}} \rangle}. \end{aligned} \quad (\text{A4})$$

Hence, the intrinsic momentum can be represented in terms of the total and center-of-mass wave function as

$$\begin{aligned} n^{\text{Int}}(\mathbf{a}) &= \left(\frac{1}{2\pi}\right)^3 \sum_{i=1}^N \int d^3\mathbf{r} e^{-i\mathbf{a}\cdot\mathbf{r}} \frac{\langle \Phi^{\text{Tot}} | e^{i\mathbf{k}_i\cdot\mathbf{r}} | \Phi^{\text{Tot}} \rangle}{\langle \Phi^{\text{Tot}} | \Phi^{\text{Tot}} \rangle} \\ &\quad \cdot (\tilde{n}_G)^{-1}, \end{aligned} \quad (\text{A5})$$

where

$$\tilde{n}_G = \frac{\langle \Phi^{\text{c.m.}} | e^{i\mathbf{k}_G\cdot\mathbf{r}/N} | \Phi^{\text{c.m.}} \rangle}{\langle \Phi^{\text{c.m.}} | \Phi^{\text{c.m.}} \rangle} = \exp\left[-\frac{1}{4b^2N}r^2\right]. \quad (\text{A6})$$

The intrinsic momentum reads

$$\begin{aligned} n^{\text{Int}}(\mathbf{a}) &= \left(\frac{b^2}{\pi\epsilon}\right)^{3/2} \sum_{i,j=1}^N \exp\left[-\frac{b^2}{\epsilon}\left[\mathbf{k} - \frac{i}{2b^2}(\mathbf{R}_i^* - \mathbf{R}_j)\right]^2\right] \\ &\quad \times B_{ij} B_{ij}^{-1}, \end{aligned} \quad (\text{A7})$$

where $\epsilon = \frac{N}{N-1}$, $B_{ij} = \langle \phi_i | \phi_j \rangle$. We note that the momentum distribution satisfies the normalization condition in N -body systems as

$$\int d\mathbf{a} n(\mathbf{a}) = N. \quad (\text{A8})$$

For ^{12}C we replace the total wave function above with the (CB-)THSR wave function:

$$\begin{aligned} |\Phi^{\text{Tot}}\rangle &\rightarrow \int d\mathbf{R}_1 d\mathbf{R}_2 d\mathbf{R}_3 \mathcal{G}_\alpha(\mathbf{R}_1, \mathbf{R}_2, \mathbf{R}_3) \\ &\quad \times |\Phi(\mathbf{R}_1)\Phi(\mathbf{R}_2)\Phi(\mathbf{R}_3)\rangle. \end{aligned} \quad (\text{A9})$$

2. Elastic form factor

For elastic collisions, the form factor is defined as

$$F(q^2) = \int d\mathbf{r} \rho_c(\mathbf{r}) e^{i\mathbf{q}\cdot\mathbf{r}}, \quad (\text{A10})$$

where q is the momentum transfer. $\rho_c(\mathbf{r})$ denotes the intrinsic charge density distribution, where ‘‘intrinsic’’ refers to the density distribution with the center-of-mass motion removed. To extract the intrinsic charge density from the total wave function, the proton charge distribution is assumed to Gaussian, and the relationship between the intrinsic matter density $\rho_m(\mathbf{r}')$ and the intrinsic charge density can be given as [64]

$$\rho_c(\mathbf{r}) = \frac{Z}{A} (\pi a_p^2)^{-\frac{3}{2}} \int d\mathbf{r}' \rho_m(\mathbf{r}') \exp\left[-\frac{(\mathbf{r}-\mathbf{r}')^2}{a_p^2}\right]. \quad (\text{A11})$$

Here, $a_p^2 = 0.43 \text{ fm}^{-2}$ represents the finite proton size [64,79]. The form factor can be read as

$$\begin{aligned} F(q^2) &= \int d\mathbf{r} \rho_c(\mathbf{r}) e^{i\mathbf{q}\cdot\mathbf{r}} \\ &= \frac{1}{A} (\pi a_p^2)^{-\frac{3}{2}} \int d\mathbf{r} \int d\mathbf{r}' \rho_m(\mathbf{r}') e^{i\mathbf{q}\cdot\mathbf{r}} \\ &\quad \times \exp\left[-\frac{(\mathbf{r}-\mathbf{r}')^2}{a_p^2}\right] \\ &= \frac{1}{A} e^{-\frac{1}{4}a_p^2 q^2} \int d\mathbf{r}' \rho_m(\mathbf{r}') e^{i\mathbf{q}\cdot\mathbf{r}'}. \end{aligned} \quad (\text{A12})$$

Expanding the last exponential term into plane waves yields

$$\begin{aligned} F(q^2) &= \frac{1}{A} e^{-\frac{1}{4}a_p^2 q^2} \int d\mathbf{r}' \rho_m(\mathbf{r}') 4\pi \sum_{l=0}^{\infty} \sum_{m=-l}^l (i)^l \\ &\quad \times j_l(qr') Y_{lm}(\theta_{r'}, \phi_{r'}) Y_{lm}^*(\theta_q, \phi_q), \end{aligned} \quad (\text{A13})$$

where $j_l(qr)$ is the spherical Bessel function of order l . Switching from Cartesian to spherical coordinates, we take $l = 0, m = 0$ for the ground state of ^{12}C ,

$$\begin{aligned} F(q^2) &= \frac{4\pi}{A} e^{-\frac{1}{4}a_p^2 q^2} \int r'^2 dr' \rho_m(r') \int \sin(\theta') d\theta' \\ &\quad \times \int d\phi' \rho_m(\theta', \phi') Y_{00}(\theta_{r'}, \phi_{r'}) j_0(qr') Y_{00}^*(\theta_q, \phi_q) \\ &= \frac{4\pi}{A} \frac{1}{2\sqrt{\pi}} e^{-\frac{1}{4}a_p^2 q^2} \int dr' r'^2 \rho_m(r') j_0(qr') Y_{00}^*(\theta_q, \phi_q). \end{aligned} \quad (\text{A14})$$

To get the relationship between the form factor and radial q^2 , we average over the angular directions:

$$\begin{aligned} F(q^2) &= \frac{4\pi}{A} \frac{1}{2\sqrt{\pi}} e^{-\frac{1}{4}a_p^2 q^2} \int dr' \rho_m(r') r'^2 j_0(qr') \\ &\quad \times \int \sin(\theta_q) d\theta_q \int d\phi Y_{00}^*(\theta_q, \phi_q) \\ &= \frac{4\pi}{A} e^{-\frac{1}{4}a_p^2 q^2} \int dr' \rho_m(r') r'^2 j_0(qr'), \end{aligned} \quad (\text{A15})$$

which is used in the calculation of form factors for the (CB-)THSR wave functions in this work.

- [1] M. Freer, H. Horiuchi, Y. Kanada-En'yo, D. Lee, and U.-G. Meißner, Microscopic clustering in light nuclei, *Rev. Mod. Phys.* **90**, 035004 (2018).
- [2] B. Zhou, Y. Funaki, H. Horiuchi, and A. Tohsaki, Nonlocalized clustering and evolution of cluster structure in nuclei, *Front. Phys.* **15**, 14401 (2020).
- [3] Z. Ren and B. Zhou, Alpha-clustering effects in heavy nuclei, *Front. Phys.* **13**, 132110 (2018).
- [4] A. Tohsaki, H. Horiuchi, P. Schuck, and G. Röpke, *Colloquium: Status of α -particle condensate structure of the Hoyle state*, *Rev. Mod. Phys.* **89**, 011002 (2017).
- [5] P. Schuck, Y. Funaki, H. Horiuchi, G. Röpke, A. Tohsaki, and T. Yamada, Alpha particle clusters and their condensation in nuclear systems, *Phys. Scr.* **91**, 123001 (2016).
- [6] M. Kimura, T. Suhara, and Y. Kanada-En'yo, Antisymmetrized molecular dynamics studies for exotic clustering phenomena in neutron-rich nuclei, *Eur. Phys. J. A* **52**, 373 (2016).
- [7] Y. Funaki, H. Horiuchi, and A. Tohsaki, Cluster models from RGM to alpha condensation and beyond, *Prog. Part. Nucl. Phys.* **82**, 78 (2015).
- [8] M. Ito and K. Ikeda, Unified studies of chemical bonding structures and resonant scattering in light neutron-excess systems, $^{10,12}\text{Be}$, *Rep. Prog. Phys.* **77**, 096301 (2014).
- [9] Y. Kanada-En'yo, M. Kimura, and A. Ono, Antisymmetrized molecular dynamics and its applications to cluster phenomena, *Prog. Theor. Exp. Phys.* **2012**, 01A202 (2012).
- [10] H. Horiuchi, K. Ikeda, and K. Katō, Recent developments in nuclear cluster physics, *Prog. Theor. Phys. Suppl.* **192**, 1 (2012).
- [11] C. W. Cook, W. A. Fowler, C. C. Lauritsen, and T. Lauritsen, B^{12} , C^{12} , and the red giants, *Phys. Rev.* **107**, 508 (1957).
- [12] F. Hoyle, M. Wilson, and P. Observatories, On nuclear reactions occurring in very hot stars, I. The synthesis of elements from carbon to nickel, *Astrophys. J. Suppl. Series* **1**, 121 (1955).
- [13] W. von Oertzen, M. Freer, and Y. Kanadaenyo, Nuclear clusters and nuclear molecules, *Phys. Rep.* **432**, 43 (2006).
- [14] E. G. Adelberger, A. García, R. G. H. Robertson, K. A. Snover, A. B. Balantekin, K. Heeger, M. J. Ramsey-Musolf, D. Bemmerer, A. Junghans, C. A. Bertulani, J.-W. Chen, H. Costantini, P. Prati, M. Couder, E. Uberseder, M. Wiescher, R. Cyburt, B. Davids, S. J. Freedman, M. Gai *et al.*, Solar fusion cross sections, II. The pp chain and CNO cycles, *Rev. Mod. Phys.* **83**, 195 (2011).
- [15] R. Bijker and F. Iachello, Evidence for triangular D'_{3h} symmetry in ^{13}C , *Phys. Rev. Lett.* **122**, 162501 (2019).
- [16] T. Yamada and Y. Funaki, Cluster states and alpha particle condensation in ^{13}C , *Int. J. Mod. Phys. E* **17**, 2101 (2008).
- [17] T. Yamada and Y. Funaki, α -cluster structures and monopole excitations in ^{13}C , *Phys. Rev. C* **92**, 034326 (2015).
- [18] N. Itagaki, T. Otsuka, K. Ikeda, and S. Okabe, Equilateral-triangular shape in ^{14}C , *Phys. Rev. Lett.* **92**, 142501 (2004).
- [19] N. Itagaki, W. von Oertzen, and S. Okabe, Linear-chain structure of three α clusters in ^{13}C , *Phys. Rev. C* **74**, 067304 (2006).
- [20] T. Suhara and Y. Kanada-En'yo, Be - α correlations in the linear-chain structure of C isotopes, *Phys. Rev. C* **84**, 024328 (2011).
- [21] N. Furutachi and M. Kimura, Bent three- α linear-chain structure of ^{13}C , *Phys. Rev. C* **83**, 021303(R) (2011).
- [22] S. Shin, B. Zhou, and M. Kimura, Shape of ^{13}C studied by the real-time evolution method, *Phys. Rev. C* **103**, 054313 (2021).
- [23] V. Della Rocca, R. Bijker, and F. Iachello, Single-particle levels in cluster potentials, *Nucl. Phys. A* **966**, 158 (2017).
- [24] D. J. Marín-Lámbarri, R. Bijker, M. Freer, M. Gai, T. Kokalova, D. J. Parker, and C. Wheldon, Evidence for triangular D_{3h} symmetry in ^{12}C , *Phys. Rev. Lett.* **113**, 012502 (2014).
- [25] D. M. Brink, History of cluster structure in nuclei, *J. Phys.: Conf. Ser.* **111**, 012001 (2008).
- [26] N. Itagaki, S. Okabe, K. Ikeda, and I. Tanihata, Molecular-orbital structure in neutron-rich C isotopes, *Phys. Rev. C* **64**, 014301 (2001).
- [27] N. Itagaki and S. Okabe, Molecular orbital structures in ^{10}Be , *Phys. Rev. C* **61**, 044306 (2000).
- [28] N. Itagaki, S. Hirose, T. Otsuka, S. Okabe, and K. Ikeda, Triaxial deformation in ^{10}Be , *Phys. Rev. C* **65**, 044302 (2002).
- [29] N. Itagaki, S. Aoyama, S. Okabe, and K. Ikeda, Cluster-shell competition in light nuclei, *Phys. Rev. C* **70**, 054307 (2004).
- [30] Y. Kanada-En'yo, Deformation of C isotopes, *Phys. Rev. C* **71**, 014310 (2005).
- [31] Y. Kanada-En'yo, M. Kimura, and H. Horiuchi, Cluster structure in stable and unstable nuclei, *Eur. Phys. J. A* **25**, 305 (2005).
- [32] Y. Kanada-En'yo and K. Ogata, Cluster structures and monopole transitions of ^{14}C , *Phys. Rev. C* **101**, 014317 (2020).
- [33] H. Masui and N. Itagaki, Simplified modeling of cluster-shell competition in carbon isotopes, *Phys. Rev. C* **75**, 054309 (2007).
- [34] T. Baba and M. Kimura, Structure and decay pattern of the linear-chain state in ^{14}C , *Phys. Rev. C* **94**, 044303 (2016).
- [35] T. Baba and M. Kimura, Coulomb shift in the mirror pair of ^{14}C and ^{14}O as a signature of the linear-chain structure, *Phys. Rev. C* **99**, 021303(R) (2019).
- [36] Y. Chiba and M. Kimura, Hoyle-analog state in ^{13}C studied with antisymmetrized molecular dynamics, *Phys. Rev. C* **101**, 024317 (2020).
- [37] Q. Zhao, Y. Suzuki, J. He, B. Zhou, and M. Kimura, α clustering and neutron-skin thickness of carbon isotopes, *Eur. Phys. J. A* **57**, 157 (2021).
- [38] A. Tohsaki, H. Horiuchi, P. Schuck, and G. Röpke, Alpha cluster condensation in ^{12}C and ^{16}O , *Phys. Rev. Lett.* **87**, 192501 (2001).
- [39] Y. Funaki, H. Horiuchi, A. Tohsaki, P. Schuck, and G. Röpke, Description of ^8Be as deformed gas-like two-alpha-particle states, *Prog. Theor. Phys.* **108**, 297 (2002).
- [40] Y. Funaki, A. Tohsaki, H. Horiuchi, P. Schuck, and G. Röpke, Analysis of previous microscopic calculations for the second 0^+ state in ^{12}C in terms of 3- α particle Bose-condensed state, *Phys. Rev. C* **67**, 051306(R) (2003).
- [41] Y. Funaki, T. Yamada, A. Tohsaki, H. Horiuchi, G. Röpke, and P. Schuck, Microscopic study of 4 α -particle condensation with inclusion of resonances, *Phys. Rev. C* **82**, 024312 (2010).
- [42] B. Zhou, Y. Funaki, H. Horiuchi, Z. Ren, G. Röpke, P. Schuck, A. Tohsaki, C. Xu, and T. Yamada, Nonlocalized clustering: A new concept in nuclear cluster structure physics, *Phys. Rev. Lett.* **110**, 262501 (2013).
- [43] M. Lyu, Z. Ren, B. Zhou, Y. Funaki, H. Horiuchi, G. Röpke, P. Schuck, A. Tohsaki, C. Xu, and T. Yamada, Investigation of ^9Be from a nonlocalized clustering concept, *Phys. Rev. C* **91**, 014313 (2015).
- [44] M. Lyu, Z. Ren, B. Zhou, Y. Funaki, H. Horiuchi, G. Röpke, P. Schuck, A. Tohsaki, C. Xu, and T. Yamada, Investigation of ^{10}Be and its cluster dynamics with the nonlocalized clustering approach, *Phys. Rev. C* **93**, 054308 (2016).

- [45] M. Lyu, K. Yoshida, Y. Kanada-En'yo, and K. Ogata, Direct probing of the cluster structure in ^{12}Be via the α -knockout reaction, *Phys. Rev. C* **99**, 064610 (2019).
- [46] Q. Zhao, Z. Ren, M. Lyu, H. Horiuchi, Y. Funaki, G. Röpke, P. Schuck, A. Tohsaki, C. Xu, T. Yamada, and B. Zhou, Investigation of the ^9Be nucleus and its cluster-nucleon correlations, *Phys. Rev. C* **97**, 054323 (2018).
- [47] Q. Zhao, Z. Ren, M. Lyu, H. Horiuchi, Y. Kanada-En'yo, Y. Funaki, G. Röpke, P. Schuck, A. Tohsaki, C. Xu, T. Yamada, and B. Zhou, Investigation of isospin-triplet and isospin-singlet pairing in the $A = 10$ nuclei ^{10}B , ^{10}Be , and ^{10}C with an extension of the Tohsaki-Horiuchi-Schuck-Röpke wave function, *Phys. Rev. C* **100**, 014306 (2019).
- [48] S. Lei, S. Li, Q. Zhao, N. Wan, M. Lyu, Z. Ren, H. Horiuchi, G. Röpke, P. Schuck, A. Tohsaki, C. Xu, and B. Zhou, Investigating the proton-halo structure of ^8B via the extended THSR wave function, *Eur. Phys. J. A* **58**, 58 (2022).
- [49] Y. Funaki, A. Tohsaki, H. Horiuchi, P. Schuck, and G. Röpke, Resonance states in ^{12}C and α -particle condensation, *Eur. Phys. J. A* **24**, 321 (2005).
- [50] Y. Funaki, H. Horiuchi, W. von Oertzen, G. Röpke, P. Schuck, A. Tohsaki, and T. Yamada, Concepts of nuclear α -particle condensation, *Phys. Rev. C* **80**, 064326 (2009).
- [51] Y. Funaki, Hoyle band and α condensation in ^{12}C , *Phys. Rev. C* **92**, 021302(R) (2015).
- [52] B. Zhou, Y. Funaki, H. Horiuchi, Z. Ren, G. Röpke, P. Schuck, A. Tohsaki, C. Xu, and T. Yamada, Nonlocalized cluster dynamics and nuclear molecular structure, *Phys. Rev. C* **89**, 034319 (2014).
- [53] T. Suhara, Y. Funaki, B. Zhou, H. Horiuchi, and A. Tohsaki, One-dimensional α condensation of α -linear-chain states in ^{12}C and ^{16}O , *Phys. Rev. Lett.* **112**, 062501 (2014).
- [54] M. Milin and W. von Oertzen, Search for molecular bands in ^{13}C , *Eur. Phys. J. A* **14**, 295 (2002).
- [55] N. Soić, M. Freer, L. Donadille, N. M. Clarke, P. J. Leask, W. N. Catford, K. L. Jones, D. Mahboub, B. R. Fulton, B. J. Greenhalgh, D. L. Watson, and D. C. Weissler, ^4He decay of excited states in ^{14}C , *Phys. Rev. C* **68**, 014321 (2003).
- [56] W. von Oertzen, H. G. Bohlen, M. Milin, T. Kokalova, S. Thummerer, A. Tumino, R. Kalpakchieva, T. N. Massey, Y. Eisermann, G. Graw, T. Faestermann, R. Hertenberger, and H.-F. Wirth, Search for cluster structure of excited states in ^{14}C , *Eur. Phys. J. A* **21**, 193 (2004).
- [57] W. von Oertzen, Chain states in ^{13}C and ^{14}C , nuclear polymers, *Nucl. Phys. A* **738**, 264 (2004).
- [58] B. Zhou, Y. Funaki, A. Tohsaki, H. Horiuchi, and Z. Ren, The container picture with two-alpha correlation for the ground state of ^{12}C , *Prog. Theor. Exp. Phys.* **2014**, 101D01 (2014).
- [59] Y. Kanada-En'yo, Variation after angular momentum projection for the study of excited states based on antisymmetrized molecular dynamics, *Phys. Rev. Lett.* **81**, 5291 (1998).
- [60] N. Takigawa and A. Arima, Structure of ^{12}C , *Nucl. Phys. A* **168**, 593 (1971).
- [61] N. Itagaki, H. Matsuno, and A. Tohsaki, Explicit inclusion of the spin-orbit contribution in the Tohsaki-Horiuchi-Schuck-Röpke wave function, *Phys. Rev. C* **98**, 044306 (2018).
- [62] T. Otsuka, T. Abe, T. Yoshida, Y. Tsunoda, N. Shimizu, N. Itagaki, Y. Utsuno, J. Vary, P. Maris, and H. Ueno, α -clustering in atomic nuclei from first principles with statistical learning and the Hoyle state character, *Nat. Commun.* **13**, 2234 (2022).
- [63] E. Uegaki, Y. Abe, S. Okabe, and H. Tanaka, Structure of the excited states in ^{12}C , *Prog. Theor. Phys.* **62**, 1621 (1979).
- [64] M. Kamimura, Transition densities between the 0_1^+ , 2_1^+ , 4_1^+ , 0_2^+ , 2_2^+ , 1_1^- , and 3_1^- states in ^{12}C derived from the three-alpha resonating-group wave functions, *Nucl. Phys. A* **351**, 456 (1981).
- [65] H. Horiuchi, Many-cluster problem by the orthogonality condition model: General discussion and ^{12}C problem, *Prog. Theor. Phys.* **53**, 447 (1975).
- [66] N. Itagaki, H. Masui, M. Ito, and S. Aoyama, Simplified modeling of cluster-shell competition, *Phys. Rev. C* **71**, 064307 (2005).
- [67] N. Itagaki, H. Masui, M. Ito, S. Aoyama, and K. Ikeda, Simplified method to include the tensor contribution in α -cluster model, *Phys. Rev. C* **73**, 034310 (2006).
- [68] N. Itagaki, Consistent description of ^{12}C and ^{16}O using a finite-range three-body interaction, *Phys. Rev. C* **94**, 064324 (2016).
- [69] T. Yoshida, N. Itagaki, and T. Otsuka, Appearance of cluster states in ^{13}C , *Phys. Rev. C* **79**, 034308 (2009).
- [70] N. Itagaki and A. Tohsaki, Improved version of a simplified method for including tensor effects in cluster models, *Phys. Rev. C* **97**, 014304 (2018).
- [71] T. Myo, H. Toki, K. Ikeda, H. Horiuchi, T. Suhara, M. Lyu, M. Isaka, and T. Yamada, High-momentum antisymmetrized molecular dynamics compared with tensor-optimized shell model for strong tensor correlation, *Prog. Theor. Exp. Phys.* **2017**, 111D01 (2017).
- [72] M. Lyu, T. Myo, M. Isaka, H. Toki, K. Ikeda, H. Horiuchi, T. Suhara, and T. Yamada, Tensor-optimized high-momentum antisymmetrized molecular dynamics with a bare interaction, and its application to the ^4He nucleus, *Phys. Rev. C* **98**, 064002 (2018).
- [73] N. Itagaki, S. Okabe, and K. Ikeda, Important role of the spin-orbit interaction in forming the $1/2^+$ orbital structure in Be isotopes, *Phys. Rev. C* **62**, 034301 (2000).
- [74] H. Horiuchi and K. Ikeda, Cluster model of the nucleus, in *Cluster Models and Other Topics*, International Review of Nuclear Physics Vol. 4 (World Scientific, Singapore, 1987), pp. 1–258.
- [75] N. Itagaki, A. Kobayakawa, and S. Aoyama, New description of light nuclei by extending the AMD approach, *Phys. Rev. C* **68**, 054302 (2003).
- [76] R. Kanungo, W. Horiuchi, G. Hagen, G. R. Jansen, P. Navratil, F. Ameil, J. Atkinson, Y. Ayyad, D. Cortina-Gil, I. Dillmann, A. Estradé, A. Evdokimov, F. Farinon, H. Geissel, G. Guastalla, R. Janik, M. Kimura, R. Knöbel, J. Kurciewicz, Y. A. Litvinov *et al.*, Proton distribution radii of $^{12-19}\text{C}$ illuminate features of neutron halos, *Phys. Rev. Lett.* **117**, 102501 (2016).
- [77] S. Li, T. Myo, Q. Zhao, H. Toki, H. Horiuchi, C. Xu, J. Liu, M. Lyu, and Z. Ren, Evolution of clustering structure through the momentum distributions in ^{8-10}Be isotopes, *Phys. Rev. C* **101**, 064307 (2020).
- [78] L. Wang, Q. Niu, J. Zhang, J. Liu, and Z. Ren, New extended method for ψ' scaling function of inclusive electron scattering, *Sci. China Phys. Mech. Astron.* **66**, 102011 (2023).
- [79] Y. Funaki, A. Tohsaki, H. Horiuchi, P. Schuck, and G. Röpke, Inelastic form factors to alpha-particle condensate states in ^{12}C and ^{16}O : What can we learn? *Eur. Phys. J. A* **28**, 259 (2006).